Small Vibrations Superimposed on a Prescribed Rigid Body Motion

A.L. SCHWAB and J.P. MEIJAARD
*Laboratory for Engineering Mechanics, Delft University of Technology, Mekelweg 2,
2628 CD Delft, The Netherlands; E-mail: a.l.schwab@wbmt.tudelft.nl*

Abstract. A method for analysing flexible multibody systems in which the elastic deformations are small is presented. The motion is considered a gross non-linear rigid body motion with small linear vibrations superimposed on it. For periodic gross motion, this results in a system of rheo-linear differential equations for the deformations with periodic coefficients. The determination of the required equations with a program for flexible multibody systems is discussed which calculates, besides the periodic gross motion, the linearized, or variational, equations of motion. Periodic solutions are determined with a harmonic balance method, while transient solutions are obtained by an averaging method. The stability of the periodic solutions is considered. The procedure has a high computational efficiency and leads to more insight into the structure of solutions. The method is applied to a pendulum with an elliptical motion of its support point, a slider-crank mechanism with flexible connecting rod, a rotor system, and a Cardan drive shaft with misalignment.

Key words: periodic solutions, non-linear vibrations, rheolinear vibrations, flexible multibody systems, general purpose software.

1. Introduction

A number of formalisms for deriving the equations of motion of rigid and flexible multibody systems are available [1, 2] and have nowadays been implemented in computer codes [3]. With these codes it is possible to make simulations of the motion of the systems under consideration. The simulation is made by numerical integration of the equations of motion, that is, by performing a transient analysis with a specific set of initial conditions.

For many applications to engineering problems a model in which all structural elements are rigid suffices for a quick judgement about the motion and forces in a system. In cases where a high accuracy is required, for instance in positioning mechanisms, or the structural elements are rather compliant, vibrations due to deformation can become important and have to be considered. Incorporation of these deformations in the dynamic analysis of the system enlarges the number of degrees of freedom, the frequency range of interest and the stiffness of the differential equations, which results in a longer simulation time.

The basic idea presented in this article is to superimpose small linear vibrations on a prescribed nominal rigid body motion. This idea is inspired by computational results from simulations of flexible multibody systems where one often recognizes a gross rigid motion with small-amplitude nearly harmonic vibrations added. This idea can at least be traced back to Cleghorn et al. [4].

The method of superimposition as presented here leads to systems of linear differential equations with time-varying coefficients. In particular, if the gross nominal motion is periodic, the coefficients are also periodic. The structure of the solutions of the equations with periodic coefficients is given by the Floquet theory [5]. Most books on this subject, for instance Yakubovich and Starzhinskii [6], deal almost exclusively with the homogeneous system and the determination of boundaries of regions of stable solutions in a parameter space. The book by Bolotin [7] is more directed towards applications in mechanics and includes a discussion of forced systems and the influence of non-linear terms, as is relevant to the subject of the present study.

Overviews of some of the numerical methods for analysing the systems are given by Friedmann [8] and Aannaque et al. [9]. We propose to use a harmonic balance method for determining periodic solutions, a kind of averaging method for transient solutions and a method directly based on the Floquet theory for stability analysis.

There are several ways to interpret the superimposition procedure. It can be seen as a first step in a regular perturbation expansion of the solution, or as a first step in an iterative solution procedure as proposed by Ling and Wu [10] and applied by Cardona et al. [11]. Our main point of view is that it should be interpreted as a first step of a Newton–Kantorovich method [12]. This method has the advantage that no small parameter has to be identified in advance and that it is robust, so in each step the linearization and the solution of the linearized problem has only to be carried out to a certain precision and remaining errors can be accounted for in the next step. Quadratic convergence is guaranteed if the initial approximation is sufficiently close to a solution, the non-linearity is small and the linear operator is not nearly singular.

The article is organized as follows. In Section 2 the formulation of the equations of motion for multibody systems is summarized for the flexible non-linear model, for the rigid model and for the linearized small vibration model. The solution techniques for the small vibrations are discussed in Section 3, where we distinguish between the periodic and transient solution, and give a method for determining the stability. Finally in Section 4, four examples are presented: first, a pendulum with prescribed elliptic motion of its support point, which leads to a forced Mathieu equation; second, a slider-crank mechanism with flexible connecting rod; third, a rotor dynamic system with isotropic bearings; and fourth, the dynamic analysis of a flexible drive shaft connected by two universal joints.

An outline of the methods has been presented earlier [13]. Here, the solution techniques are explained in more detail and applications to planar as well as spatial systems are given.

2. Equations of Motion

The equations of motion are derived with the formalism that has been developed at our institute [14–16], which has been implemented in a program called SPACAR [17]. The formalism is based on a finite element method for modelling and analysing the motion of planar and spatial multibody systems with rigid and flexible links. With the help of a rather limited number of element types it is possible to model a wide class of systems. Typical types of elements are beam, truss and hinge elements, while more specialized elements can be used to model joint connections and transmissions of motion.

2.1. GENERAL FLEXIBLE MODEL

In a finite element description of a multibody system the configuration is described by a number of nodal points with coordinates $\mathbf{x}$ and a number of elements with deformation mode coordinates $\boldsymbol{\epsilon}$. The deformation mode coordinates depend on the nodal coordinates and can be expressed as $\boldsymbol{\epsilon} = \mathbf{D}(\mathbf{x})$. Usually constraints are imposed on some deformation modes and nodal coordinates, which we assume, for the present context, to be holonomic. For instance, the conditions for rigidity of element e are $\boldsymbol{\epsilon}^e = \mathbf{D}^e(\mathbf{x}^e) = \mathbf{0}$. If the constraints are consistent, the coordinates can locally be expressed as functions of the generalized coordinates $\mathbf{q}$, the kinematic degrees of freedom (configuration coordinates), by means of a transfer function $\mathbf{F}$ as

$$\mathbf{x} = \mathbf{F}(\mathbf{q}). \tag{1}$$

The generalized coordinates can be chosen from components of the nodal coordinate vector $\mathbf{x}$ and the deformation mode vector $\boldsymbol{\epsilon}$. For large motions a change of generalized coordinates may sometimes be necessary. Generally the transfer function cannot be calculated explicitly, but has to be determined by solving the constraint equations in an iterative way. Derivatives are calculated by means of implicit differentiation.

For each node and element, we determine a mass matrix $\mathbf{M}^e$ and a force vector $\mathbf{f}^e$, which give a contribution to the virtual power of $\delta \dot{\mathbf{x}}^{eT} (\mathbf{f}^e - \mathbf{M}^e \ddot{\mathbf{x}}^e)$. The unreduced equations of motion are obtained by assembling the contribution of all elements and nodes in a global mass matrix $\mathbf{M}$ and a global force vector $\mathbf{f}$, which results in

$$\delta \dot{\mathbf{x}}^T [\mathbf{f}(\dot{\mathbf{x}}, \mathbf{x}, t) - \mathbf{M}(\mathbf{x})\ddot{\mathbf{x}}] = 0. \tag{2}$$

Here, $\delta \dot{\mathbf{x}}$ are kinematically admissible virtual velocities, which satisfy all instantaneous kinematic constraints. The degrees of freedom can be split in prescribed

ones, $\mathbf{q}^r$, which are known explicit functions of time and represent the rheonomic constraints, which are the prescribed input motions, and the dynamic degrees of freedom $\mathbf{q}^d$. By differentiating the transfer function (1) we obtain

$$\dot{\mathbf{x}} = \mathbf{F}_{,\mathbf{q}}\dot{\mathbf{q}}, \quad \ddot{\mathbf{x}} = \mathbf{F}_{,\mathbf{q}}\ddot{\mathbf{q}} + \mathbf{F}_{,\mathbf{qq}}\dot{\mathbf{q}}\dot{\mathbf{q}}, \quad \delta\dot{\mathbf{x}} = \mathbf{F}_{,\mathbf{q}^d}\delta\dot{\mathbf{q}}^d. \tag{3}$$

Here a subscript comma followed by one or more variables denotes partial derivatives with respect to these variables. The way in which higher-order derivatives have to be multiplied by the juxtaposed vectors goes without saying. Substituting these expressions in the virtual power equation (2) yields the reduced equations of motion in state space form

$$\bar{\mathbf{M}}(\mathbf{q}^d, t)\ddot{\mathbf{q}}^d = \bar{\mathbf{f}}(\dot{\mathbf{q}}^d, \mathbf{q}^d, t), \tag{4}$$

with the reduced global mass matrix,

$$\bar{\mathbf{M}} = \mathbf{F}_{,\mathbf{q}^d}^T \mathbf{M} \mathbf{F}_{,\mathbf{q}^d}, \tag{5}$$

and the reduced global force vector,

$$\bar{\mathbf{f}} = \mathbf{F}_{,\mathbf{q}^d}^T [-\mathbf{M}(\mathbf{F}_{,\mathbf{qq}}\dot{\mathbf{q}}\dot{\mathbf{q}} + \mathbf{F}_{,\mathbf{q}^r}\ddot{\mathbf{q}}^r) + \mathbf{f}]. \tag{6}$$

Details are given by Jonker [15].

2.2. NOMINAL GROSS MOTION

The state in which all elements are rigid is chosen as a nominal solution. The input motions $\mathbf{q}^r$ are prescribed periodic functions of time and the dynamic degrees of freedom, $\mathbf{q}^d$, which describe the deformations, are identically equal to zero. In order to maintain these prescribed values for the deformations, additional forces, $\mathbf{f}^d$, dual to the deformation modes $\mathbf{q}^d$ have to be introduced in the right-hand side of the reduced equations of motion (4) and the sum of all reduced forces has to be zero,

$$\mathbf{F}_{,\mathbf{q}^d}^T [-\mathbf{M}(\mathbf{F}_{,\mathbf{q}^r\mathbf{q}^r}\dot{\mathbf{q}}^r\dot{\mathbf{q}}^r + \mathbf{F}_{,\mathbf{q}^r}\ddot{\mathbf{q}}^r) + \mathbf{f}] + \mathbf{f}^d = \mathbf{0}. \tag{7}$$

From this equation the additional forces $\mathbf{f}^d$ are found.

2.3. LINEARIZED EQUATIONS FOR SMALL VIBRATIONS

To describe the small vibration we have to linearize the equations of motion about the nominal solution in which the deformation mode coordinates $\mathbf{q}^d$ are zero. Linearizing the reduced equation of motion (4) at $\mathbf{q}^d = \mathbf{0}$, $\dot{\mathbf{q}}^d = \mathbf{0}$ and $\ddot{\mathbf{q}}^d = \mathbf{0}$ results in

$$\bar{\mathbf{M}}\Delta\ddot{\mathbf{q}}^d + \bar{\mathbf{C}}\Delta\dot{\mathbf{q}}^d + \bar{\mathbf{K}}\Delta\mathbf{q}^d = -\mathbf{f}^d + \mathbf{f}_a^d. \tag{8}$$

Here $\bar{\mathbf{M}}$ is the system mass matrix from (5), $\bar{\mathbf{C}}$ is the velocity sensitivity matrix and $\bar{\mathbf{K}}$ contains the stiffness terms; $\mathbf{f}^d$ are the forces from (7) and $\mathbf{f}_a^d$ represent additional applied forces that are not included in the calculation of the nominal solution. These arise from independently modelled elements or subsystems, for instance actuators with a control system or bearings and seals in rotor dynamics. $\bar{\mathbf{M}}$ is symmetric, but $\bar{\mathbf{C}}$ and $\bar{\mathbf{K}}$ need not.

The matrices of the linearized equations are determined in the following way. First, for all elements and nodes the contribution to the global stiffness matrix $\mathbf{K}$ and the global velocity matrix $\mathbf{C}$ are determined as

$$\mathbf{C}^e = -(\mathbf{f}^e)_{,\dot{\mathbf{x}}^e}, \quad \mathbf{K}^e = (\mathbf{M}^e \ddot{\mathbf{x}}^e - \mathbf{f}^e)_{,\mathbf{x}^e}. \tag{9}$$

These global matrices having been determined, the matrices in the linearized equations are given by

$$\begin{aligned}
\bar{\mathbf{C}} &= \mathbf{F}_{,\mathbf{q}^d}^T \mathbf{C} \mathbf{F}_{,\mathbf{q}^d} + 2\mathbf{F}_{,\mathbf{q}^d}^T \mathbf{M} \mathbf{F}_{,\mathbf{q}^d\mathbf{q}} \dot{\mathbf{q}}, \\
\bar{\mathbf{K}} &= \mathbf{F}_{,\mathbf{q}^d}^T \mathbf{K} \mathbf{F}_{,\mathbf{q}^d} + \mathbf{F}_{,\mathbf{q}^d\mathbf{q}^d}^T [\mathbf{M}\ddot{\mathbf{x}} - \mathbf{f}] \\
&\quad + \mathbf{F}_{,\mathbf{q}^d}^T [\mathbf{M}(\mathbf{F}_{,\mathbf{q}^d\mathbf{q}}\ddot{\mathbf{q}} + \mathbf{F}_{,\mathbf{q}^d\mathbf{q}\mathbf{q}}\dot{\mathbf{q}}\dot{\mathbf{q}}) + \mathbf{C}\mathbf{F}_{,\mathbf{q}^d\mathbf{q}}\dot{\mathbf{q}}].
\end{aligned} \tag{10}$$

The kinematics and statics of an independently modelled element e can be determined from the transfer functions and the degrees of freedom as

$$\begin{aligned}
\Delta\mathbf{x}^e &= \mathbf{F}_{,\mathbf{q}^d}^e \Delta\mathbf{q}^d, \\
\Delta\dot{\mathbf{x}}^e &= \mathbf{F}_{,\mathbf{q}^d}^e \Delta\dot{\mathbf{q}}^d + \mathbf{F}_{,\mathbf{q}^d\mathbf{q}}^e \dot{\mathbf{q}}\Delta\mathbf{q}^d, \\
\Delta\ddot{\mathbf{x}}^e &= \mathbf{F}_{,\mathbf{q}^d}^e \Delta\ddot{\mathbf{q}}^d + 2\mathbf{F}_{,\mathbf{q}^d\mathbf{q}}^e \dot{\mathbf{q}}\Delta\dot{\mathbf{q}}^d + \mathbf{F}_{,\mathbf{q}^d\mathbf{q}\mathbf{q}}^e \dot{\mathbf{q}}\dot{\mathbf{q}}\Delta\mathbf{q}^d,
\end{aligned} \tag{11}$$

from which the relative displacements, velocities and accelerations can be determined. The additional reduced forces $\mathbf{f}_a^{de}$ follow from linearized constitutive equations and inertia terms as

$$\mathbf{f}_a^{de} = \mathbf{F}_{,\mathbf{q}^d}^{eT}(-\mathbf{K}^e \Delta\mathbf{x}^e - \mathbf{C}^e \Delta\dot{\mathbf{x}}^e - \mathbf{M}^e \Delta\ddot{\mathbf{x}}^e + \mathbf{f}^e), \tag{12}$$

which gives contributions to the total reduced mass, velocity sensitivity and stiffness matrices and right-hand side of the linearized equations.

The resulting set of linearized equations is amenable to several kinds of analysis, such as the determination of stationary and periodic solutions, the investigation of the stability of these solutions and the continuation of these solutions if a parameter, for instance the driving speed of a mechanism, is varied [16, 18]. Model reduction methods can be applied in addition.

3. Solution Techniques for Small Vibrations

The complete solution consists of the nominal gross rigid body motion, and a periodic solution and a transient of the linearized equations superimposed on it.

Our main objective is the periodic solution of the small vibrations. In this section, approximate methods for finding the periodic and transient solution for the small vibrations and a method for determining their stability will be discussed.

3.1. PERIODIC SOLUTION

The starting point for the periodic solution of the small vibration is the linearized equation (8) with the excitation $-\mathbf{f}^d$, left over from the nominal solution, on the right-hand side

$$\bar{\mathbf{M}}(t_i)\Delta\ddot{\mathbf{q}}^d + \bar{\mathbf{C}}(t_i)\Delta\dot{\mathbf{q}}^d + \bar{\mathbf{K}}(t_i)\Delta\mathbf{q}^d = -\mathbf{f}^d(t_i). \tag{13}$$

Additional forces $\mathbf{f}_a^d$ are assumed to have been absorbed in $-\mathbf{f}^d$ if they are present. Here t_i denote the discrete times with $i = 0, \ldots, p$ and p being the total number of discrete positions in which the system is calculated. The period of the system is $T = (t_p - t_0) = 2\pi/\omega$.

As a periodic solution of these equations we propose a truncated Fourier series for $\Delta\mathbf{q}^d$ with the same fundamental frequency ω as the nominal gross motion,

$$\Delta\mathbf{q}^d = \sum_{l=-m}^{m} \Delta\tilde{\mathbf{q}}_l^d\, \mathrm{e}^{il\omega t}. \tag{14}$$

Here m is the number of frequencies that is expected to determine the solution to the required accuracy, which is usually much less than $p/2$. The unknown coefficients $\Delta\tilde{\mathbf{q}}_l^d$ are calculated as follows. First, the linearized equation (8) is transformed for every discrete moment in time as

$$\Delta\ddot{\mathbf{q}}^d + \mathbf{P}(t_i)\Delta\dot{\mathbf{q}}^d + \mathbf{Q}(t_i)\Delta\mathbf{q}^d = \mathbf{r}(t_i), \tag{15}$$

with

$$\begin{aligned}
\mathbf{P}(t_i) &= \bar{\mathbf{M}}^{-1}(t_i)\bar{\mathbf{C}}(t_i), \\
\mathbf{Q}(t_i) &= \bar{\mathbf{M}}^{-1}(t_i)\bar{\mathbf{K}}(t_i), \\
\mathbf{r}(t_i) &= -\bar{\mathbf{M}}^{-1}(t_i)\mathbf{f}^d(t_i).
\end{aligned} \tag{16}$$

Second, the coefficients of this equation are transformed into Fourier series as

$$\Delta\ddot{\mathbf{q}}^d + \left(\sum_k \tilde{\mathbf{P}}_k\, \mathrm{e}^{ik\omega t}\right)\Delta\dot{\mathbf{q}}^d + \left(\sum_k \tilde{\mathbf{Q}}_k\, \mathrm{e}^{ik\omega t}\right)\Delta\mathbf{q}^d = \sum_k \tilde{\mathbf{r}}_k\, \mathrm{e}^{ik\omega t}. \tag{17}$$

Here, the summation over k extends from $-(p-1)/2$ to $(p-1)/2$ for odd p and from $-(p-2)/2$ to $(p-2)/2$ for even p. Third, the truncated Fourier series for $\Delta\mathbf{q}^d$ (14) is substituted in the differential equations (17) and every individual harmonic is balanced. This means that the convolutions are determined and the coefficients

of $\exp(ik\omega t)$, $(k = -m, \ldots, m)$ on both sides of the equation are balanced. This results in a set of $(2m + 1)n$ linear equations of the form

$$\sum_l \{\tilde{\mathbf{Q}}_{k-l} - (l\omega)^2\delta_{kl}\mathbf{I} + (il\omega)\tilde{\mathbf{P}}_{k-l}\}\Delta\tilde{\mathbf{q}}_l^d = \tilde{\mathbf{r}}_k, \tag{18}$$

with n the dimension of the deformation mode coordinate vector $\Delta\mathbf{q}^d$ and k and l extend from $-m$ to m. If $k - l$ falls outside the range, the matrices $\tilde{\mathbf{Q}}_{k-l}$ and $\tilde{\mathbf{P}}_{k-l}$ are replaced by zero matrices. From this harmonic balance (18) the coefficients $\Delta\tilde{\mathbf{q}}_l^d$ can be solved. These coefficients are the harmonics of the periodic solution and tell us how each frequency is present in the response. Finally, the result can be interpreted in the time domain as in Equation (14).

3.2. TRANSIENT SOLUTION

The complete solution of the linearized equations consists of a periodic solution as determined in the previous subsection and a transient solution that is added to it in order to satisfy the initial conditions. The transient solution is constructed with the help of the method of slowly varying coefficients and averaging [20, chapter 11]. This transient solution has to satisfy the homogeneous equations corresponding to (8), which are rewritten as a system of first-order differential equations as

$$\dot{\mathbf{y}} = \mathbf{A}(t)\mathbf{y}, \quad \text{with} \quad \mathbf{y} = \begin{bmatrix} \Delta\mathbf{q}^d \\ \Delta\dot{\mathbf{q}}^d \end{bmatrix},$$

$$\mathbf{A}(t) = \begin{bmatrix} \mathbf{0} & \mathbf{I} \\ -\bar{\mathbf{M}}^{-1}(t)\bar{\mathbf{K}}(t) & -\bar{\mathbf{M}}^{-1}(t)\bar{\mathbf{C}}(t) \end{bmatrix}. \tag{19}$$

The matrix $\mathbf{A}(t)$ from (19) is periodic with period $T = 2\pi/\omega$ as stated in Section 3.1 and can be written as the sum of a constant part, $\mathbf{A}_0$, and a periodic part with average equal to zero, $\tilde{\mathbf{A}}(t)$. The differential equations are transformed on the basis of eigenvectors of the matrix $\mathbf{A}_0$, which results in

$$\dot{\mathbf{z}} = [\mathbf{J}_0 + \tilde{\mathbf{J}}(t)]\mathbf{z}, \tag{20}$$

where $\mathbf{Y}$ is the matrix of eigenvectors and

$$\mathbf{J}_0 = \mathbf{Y}^{-1}\mathbf{A}_0\mathbf{Y}, \quad \tilde{\mathbf{J}}(t) = \mathbf{Y}^{-1}\tilde{\mathbf{A}}(t)\mathbf{Y}. \tag{21}$$

If we assume that all eigenvalues of $\mathbf{A}_0$ are distinct, the matrix $\mathbf{J}_0$ is diagonal and $\tilde{\mathbf{J}}(t)$ is in general a full time dependent matrix with period T, whose entries are assumed to be small with respect to the diagonal terms of $\mathbf{J}_0$. A second transformation writes the differential equations on the basis of eigensolutions according to the diagonal matrix $\mathbf{J}_0$ with slowly varying coefficients $\mathbf{a}(t)$. With

$$\mathbf{z} = e^{\mathbf{J}_0 t}\mathbf{a}, \tag{22}$$

this results in a set of differential equations for the amplitudes $\mathbf{a}$ as

$$\dot{\mathbf{a}} = [e^{-\mathbf{J}_0 t} \tilde{\mathbf{J}}(t) \, e^{\mathbf{J}_0 t}] \mathbf{a}. \tag{23}$$

This equation is still fully equivalent to (19). Now if it is assumed that $\mathbf{J}_0$ contains only well separated damped eigenfrequencies with a corresponding period that is small in comparison with T, that is, the diagonal elements of $\mathbf{J}_0$ have negative real parts, while their imaginary parts are much larger than $\omega = 2\pi/T$, and have large differences, only the diagonal terms of $\tilde{\mathbf{J}}(t)$ yield contributions after averaging. The off-diagonal terms give rise to oscillating terms of the form $\tilde{J}_{ij} \exp[(-J_{0ii} + J_{0jj})t]$ $(i \neq j)$ which disappear in the process of averaging. The solution of the amplitudes becomes

$$a_i(t) = a_i(0) \exp\left[\int\limits_0^t \tilde{J}_{ii}(\tau) \, d\tau\right]. \tag{24}$$

Given the Fourier series of $\mathbf{A}(t)$ and of $\tilde{\mathbf{J}}(t)$, it would be tempting to try and find the Fourier series of $\mathbf{a}(t)$. Owing to the non-linear operator $\exp(\int \ldots dt)$ this is not straightforward and we propose to solve for the transient solution according to (24) and, if necessary, to calculate the Fourier series of the result.

If the assumptions are fulfilled, the first order averaging appears to have a sufficient accuracy for our application. In other cases or when a higher accuracy is required, direct numerical integration of the linearized equations can be used.

3.3. STABILITY OF THE SOLUTIONS

The stability of the solutions can be investigated by analysing the homogeneous equations. Several methods can be used. For instance, if the method of slowly varying amplitude and averaging is used, as in the previous subsection, the stability is directly determined by the eigenvalues of $\mathbf{A}_0$, as can be seen from (22) and (23). If they have all negative parts, stability is expected if the approximation is sufficiently accurate and the stability margin is sufficiently large. This method, however, is not always reliable.

Another more exact method first calculates the monodromy matrix, after which the characteristic multipliers are determined as the eigenvalues of this matrix [16, 18].

An approach is proposed here which is directly based on the theory of Floquet [5]. This theory states that the solution of the homogeneous system consists of a sum of $2n$ ($2n$ is the number of first order differential equations in (19)) fundamental solutions of the form of a periodic function multiplied by an exponential function (in the generic case of distinct characteristic multipliers). From these, the characteristic exponents and hence the stability can directly be read.

We assume fundamental solutions of the form

$$\Delta\mathbf{q}^d = \mathrm{e}^{\lambda t} \sum_{l=-m}^{m} \Delta\tilde{\mathbf{q}}_l^d \, \mathrm{e}^{il\omega t},$$ (25)

where λ is a characteristic exponent. This expression can be substituted in the homogeneous equations (13) or an equivalent system of first-order equations (19). By collecting terms with equal exponentials and equating the coefficients of $\exp(\lambda t + il\omega t)$ $(l = -m, \ldots, m)$ to zero, we obtain a set of homogeneous linear algebraic equations for the values of $\Delta\tilde{\mathbf{q}}_l^d$ as

$$\sum_l \{\lambda^2 \delta_{kl}\mathbf{I} + \lambda\mathbf{V}_{kl} + \mathbf{W}_{kl}\}\Delta\tilde{\mathbf{q}}_l^d = \mathbf{0},$$ (26)

with k and l ranging from $-m$ to m. The individual matrices in (26) with dimension $n \times n$ are given by

$$\begin{aligned}\mathbf{V}_{kl} &= \tilde{\mathbf{P}}_{k-l} + 2(il\omega)\delta_{kl}\mathbf{I}, \\ \mathbf{W}_{kl} &= \tilde{\mathbf{Q}}_{k-l} - (l\omega)^2\delta_{kl}\mathbf{I} + (il\omega)\tilde{\mathbf{P}}_{k-l}.\end{aligned}$$ (27)

Again, if $k - l$ falls outside the range, the matrices $\tilde{\mathbf{P}}_{k-l}$ and $\tilde{\mathbf{Q}}_{k-l}$ are replaced by zero matrices. Non-trivial solutions for $\Delta\tilde{\mathbf{q}}_l^d$ are only possible if the determinant of the coefficients from (26) is zero, which leads to an eigenvalue problem for the characteristic exponents λ.

Because this determinant has the degree $(2m + 1)2n$, the number of characteristic exponents obtained in this way is $(2m + 1)$ times as large as their true number. They appear in clusters of values which differ approximately by an integral multiple of $i\omega$ and correspond to the same fundamental solution. From each cluster, only the exponent that has the smallest imaginary part is considered as an approximation for the true characteristic exponent. Algorithms that calculate only a subset of the eigenvalues with the smallest absolute values [21] can be used to advantage.

This method of determining characteristic exponents can be seen as an extension of the method of truncated infinite determinants of Hill [22]. Also Bolotin [7] gives a description. Naab and Weyh [23] use a similar method.

4. Examples and Comparison

4.1. PENDULUM

As a first example of the described method a pendulum with a forced elliptic motion of its support point is considered. Especially the cases of purely vertical motion and circular motion constitute well studied problems. The system, shown in Figure 1, consists of a rigidly modelled vertical pendulum of length $l = 1.0$ [m] with a point mass at the bottom end. The top end moves on an ellipse. This path is generated by a hypocycloidal gear pair with a ratio of annulus over spur radius equal to 2.
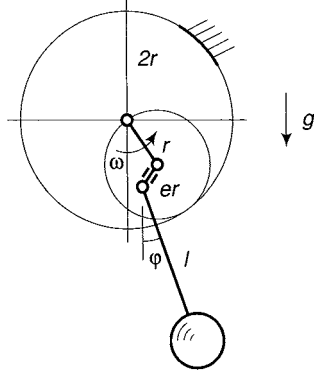
Figure 1. Pendulum with a forced elliptic motion of its support point.

This gear pair is also known as 'Cardan circles'. The top end of the pendulum is pin joined to the pinion at a distance *er* from the centre, in this way creating an ellipse with major axis $2(1 + e)r$ and minor axis $2(1 - e)r$. In this example the pinion radius *r* is taken 0.5 [m] and the eccentricity factor *e* is 0.5. A crank with a uniform angular velocity ω moves the centre of the pinion. In the joint between the pendulum and the pinion a viscous damping is assumed which results in 1% of critical damping in the linearized equations. The system operates in a gravitational field with $g = 9.81$ [N/kg]. The non-linear equation of motion is given by

$$\ddot{\varphi} + 2\zeta\omega_0(\dot{\varphi} + \omega) + \omega_0^2 \sin\varphi + \rho\omega^2[\sin(\varphi - \omega t) + e\sin(\varphi + \omega t)] = 0, \quad (28)$$

with the parameters $\rho = r/l$, the relative damping ζ and the undamped eigenfrequency of the isolated pendulum $\omega_0 = \sqrt{g/l}$. The angle φ is measured from the down-hanging vertical position. The linearized equation of motion, which describes the small vibration $\Delta\varphi$ around $\varphi = 0$, is

$$\Delta\ddot{\varphi} + 2\zeta\omega_0\Delta\dot{\varphi} + [\omega_0^2 + (1 + e)\rho\omega^2\cos\omega t]\Delta\varphi$$

$$= -2\zeta\omega_0\omega + (1 - e)\rho\omega^2\sin\omega t. \quad (29)$$

The periodic solution for $\Delta\varphi$ is assumed to be a truncated Fourier series with the fundamental frequency equal to the driving frequency ω. Notice that the periodic solution of $\Delta\varphi$ will show a non-zero mean value due to the term related to the damping $-2\zeta\omega_0\omega$ in the right-hand side of differential equation (29). A characteristic value for the periodic solution is the amplitude $\Delta\hat{\varphi}$, being $(1/2)[(\Delta\varphi)_{max} - (\Delta\varphi)_{min}]$ (half of the range of $\Delta\varphi$) over one period. This amplitude is shown in Figure 2 for a range of driving speeds ω. Resonance clearly occurs at about 1/2 of the undamped eigenfrequency ω_0. The 1/3 subresonance is just discernible. If we compare this with the full non-linear response curves, the dashed lines, we see approximately the same result; only the resonance peak bends slightly backward due to the non-linearity. The non-linear response was calculated with a shooting method as described by Meijaard [18]. Although we have shown
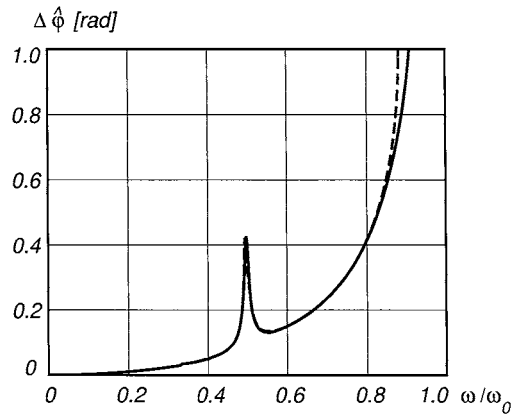
Figure 2. Amplitude $\Delta\hat{\varphi}$ for the periodic solution of the pendulum for damping $\zeta = 0.01$ in the driving speed range of $0 < \omega/\omega_0 < 0.9$. The solid line is the linearized result, the dashed line is the full non-linear result.
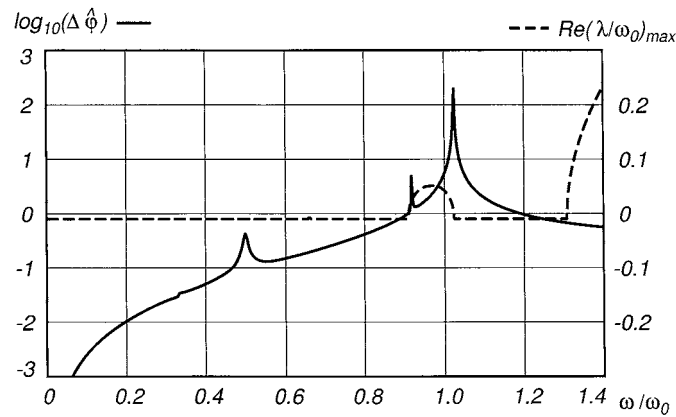

Figure 3. The solid line is the logarithmic amplitude $\Delta\hat{\varphi}$ for the periodic solution of the pendulum for damping $\zeta = 0.01$ in the driving speed range of $0 < \omega/\omega_0 < 1.4$. The dashed line is the maximum of the real part of the dimensionless characteristic exponents λ/ω_0.

the equation of motion and its linearization in an analytic form we must emphasize that all calculations presented here were done in a discrete and numeric way as described in the previous sections.

The same response on a logarithmic scale over a wider range of driving speeds together with an indication upon the stability of the periodic solution is shown in Figure 3. If the maximal real part of the characteristic exponents λ is negative, the solution is stable. From the figure we see that stable periodic solutions can be found within the ranges $0 \leq \omega/\omega_0 < 0.91$ and $1.02 < \omega/\omega_0 < 1.31$. The instabilities near $\omega/\omega_0 = 0.91$ and $\omega/\omega_0 = 1.02$ are of the transcritical type, in which a characteristic exponent becomes zero and the resonance peaks become unbounded. In the figure, the peaks remain bounded because the response was calculated for

a finite number of discrete values of ω. Near $\omega/\omega_0 = 1.31$ a Neimark–Hopf bifurcation occurs, where a pair of complex conjugated characteristic exponents cross the imaginary axis and no resonance appears. All periodic solutions within the range $0.9 < \omega/\omega_0 < 1.2$ must be discarded due to the large amplitudes which are in contradiction with the assumption of small vibrations.

4.2. SLIDER-CRANK MECHANISM

As a second and more engineering type of example a slider-crank mechanism is considered. The same mechanism has been used as an example in a series of publications by Song and Haug [24], Jonker [15] and Meijaard [18], among others. With [18] a comparison will be made.

The system consists of a rigidly modelled crank of length 0.15 [m], a flexible connecting rod of length 0.3 [m] and a plunger. The crank and the connecting rod have a uniform mass distribution of 0.2225 [kgm^{-1}], the mass of the plunger is 0.033375 [kg], the flexural rigidity of the connecting rod is $EI = 12.72345$ [Nm^2] and the centre line is assumed inextensible. The crank rotates at a constant angular velocity ω, so this system is periodically forced. Two values of material damping according to the Kelvin–Voigt model are considered, such that the damping in the connecting rod of the first eigenmode for small vibrations when the crank is fixed is 1% respectively 2% of critical damping. The connecting rod is modelled by two planar beam elements (4 dynamic degrees of freedom).

Figure 4 shows the periodic and the total, summed periodic and first period transient, response for $\omega = 150$ [rad/s] of the dimensionless lateral deflection of the centre of the connecting rod, that is, the distance of the centre point of the rod to the line connecting the endpoints divided by the reference length of the rod. The deformations and deformation rates are zero at $t = 0$ and the shown solutions correspond to the 2% damping case. If we compare the linearized results with the results from Meijaard [18] we note the good agreement. However, in the transient response we see a small difference at the start, due to non-linearity and inaccuracy in the process of averaging.

Figure 5 shows the dimensionless maximal midpoint deflection for different values of the angular velocity of the crank for the periodic solution. Resonances occur at about 1/5, 1/4 and 1/3 of the first eigenfrequency. For the numerical model of the connecting rod with pinned joints and modelled by two beam elements, this frequency is 832 [rad/s]. If we compare this with the full non-linear response curves, the dashed lines, we see that the resonance at 1/5 of the first eigenfrequency is not observed and the resonance peaks bend backwards owing to the non-linearity.

Figure 6 shows the amplitude of the first four harmonics of the periodic solutions as a function of the driving frequencies ω in the same range as Figure 5. The dotted lines show the corresponding quasistatic forcing solution, i.e. the harmonic forcing multiplied by the inverse of the average stiffness matrix. It is clearly seen that the third harmonic has a resonance peak near 1/3 of the first eigenfrequency
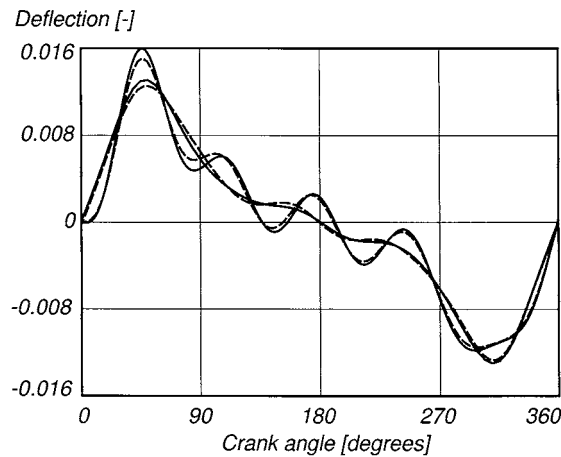
Figure 4. Dimensionless midpoint deflections of the connecting rod at ω =150 [rad/s] and a damping of 2%. The smooth curves are the periodic solutions and the oscillating curves are the sum of the periodic and the transient solutions. The drawn lines are the linearized results, the dashed lines are the full non-linear results from Meijaard [18].
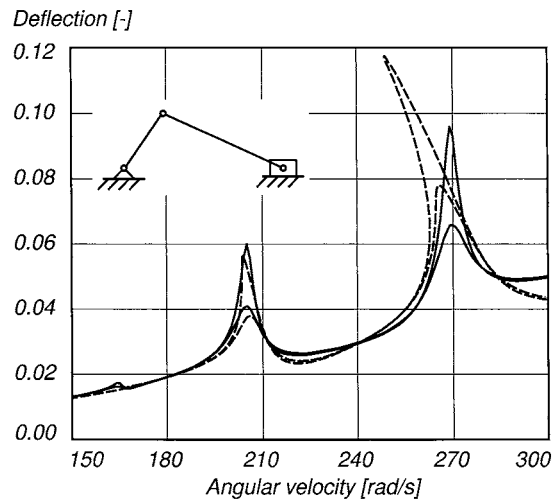

Figure 5. Maximal dimensionless midpoint deflections of the periodic solutions for 1 and 2% damping in the driving speed range of $150 < \omega < 300$ [rad/s]. The drawn lines are the linearized results, the dashed lines are the full non-linear results from Meijaard [18].

and also a secondary peak near 1/4 of this frequency. This phenomenon can be observed in nearly all harmonics. The most interesting one is the fourth harmonic, which shows a resonance peak near 1/4 of the first eigenfrequency, notwithstanding the fourth harmonic in the forcing is absent. In the non-linear analysis the lower solution around the backbones is unstable and the jump phenomenon can occur. This is not present in the small vibrations model.
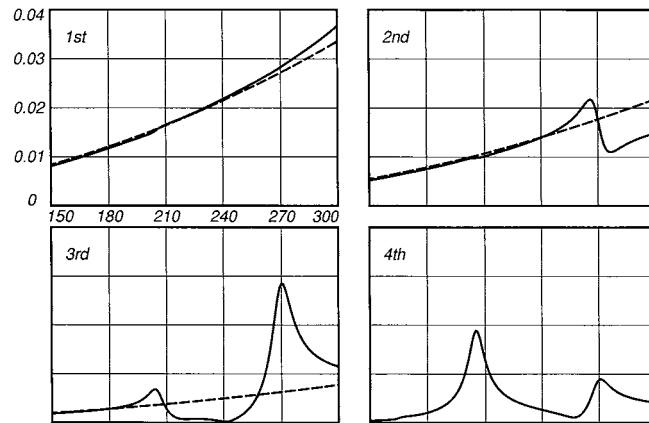
Figure 6. The amplitude scaled from 0 to 0.04 of the first four harmonics for 2% damping in the driving speed range of 150 < ω < 300 [rad/s] from Figure 5. The dotted lines show the quasistatic forcing solution.

4.3. ROTOR DYNAMICS MODEL [25]

It will be shown how the approach of this article can directly be applied to derive rotor dynamic models and to analyse their linearized behaviour. In order to assess the validity and accuracy of the models, a comparison with a problem from literature [26] is made.

By the linearization procedure the structural equations of the rotor system are obtained in a linearized form, where a splitting can be made of terms that are independent, linear, or quadratic in the rotary speed or linear in the angular acceleration. The kinematics of the additional elements such as bearings, seals, squeeze film dampers and air gaps, can be linearized in the same way, as shown in Equation (11). The constitutive equations of these elements can be added to the structural equations as explained by Equation (12). In the context of the present article, these have to be linearized. If the original non-linear model is comprehensive, all kinds of effects that give a contribution to the linearized equations, such as load-dependent terms, initial deflections, and mass unbalances, are automatically taken into account.

As the data for the example was originally given in imperial technical units, the following conversion factors have been used, where needed: 1 [in] = 0.0254 [m]; 1 [lb] = 0.45359237 [kg]; 1 [lbf] = 4.4482216 [N]; normal acceleration of gravity g_n = 9.80665 [N/kg].

The example system consists of a solid circular cylindric shaft of length 50 [in] and diameter 4 [in] made of steel with density 0.283 [lb/in^3] and modulus of elasticity 3.0 · 10^7 [lbf/in^2] (Figure 7). This shaft is supported at one end and at a position 10 [in] from the same end by isotropic bearings with stiffness 100 000 [lbf/in]. A liquid annular seal is placed 20 [in] from the same end. This seal is not
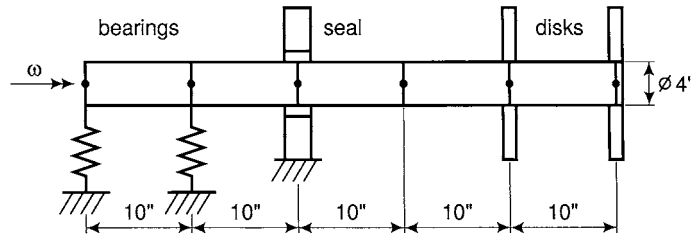
Figure 7. Rotor system consisting of a shaft, two isotropic linearly elastic bearings, a seal and two disks.

included in the calculation of the nominal solution. The additional forces exerted on the shaft are given by the linearized equations

$$\begin{bmatrix} f_y \\ f_z \end{bmatrix} = - \begin{bmatrix} K & k \\ -k & K \end{bmatrix} \begin{bmatrix} \Delta y \\ \Delta z \end{bmatrix} - \begin{bmatrix} C & c \\ -c & C \end{bmatrix} \begin{bmatrix} \Delta \dot{y} \\ \Delta \dot{z} \end{bmatrix}. \tag{30}$$

Here, f_y and f_z are the lateral forces on the shaft, Δy and Δz are the lateral displacements, and $K = 89\,542$ [lbf/in], $k = 27\,028$ [lbf/in], $C = 171.42$ [lbf s/in] and $c = 12$ [lbf s/in] are the stiffness and damping parameters of the seal. The constitutive equations are the same in a co-rotating reference frame. In addition a part of the mass of the seal, 6.68 [kg], is added to the shaft at the position of the seal. Two disks with mass 0.028 [lbf s^2/in], axial moment of inertia 0.224 [lbf s^{2}in] and transverse moment of inertia 0.114 [lbf s^{2}in] are placed at the other end and 10 [in] away from that end.

The eigenfrequencies when the shaft turns at 4000 revolutions per minute are calculated. The shaft is modelled with five finite beam elements of equal length with neglected shear deformations but with inclusion of the rotary inertia of the cross-section of the shaft. As the eigenfrequencies are determined with respect to a co-rotating frame of reference in the present study, the corresponding frequencies with respect to a stationary frame are determined by adding the rotary speed to the frequencies of forward whirling modes and subtracting this speed from the frequencies of backward whirling modes. The first eight eigenvalues are given in Table I; for comparison, the values from [26] are listed in the same table. The differences are less than one percent, despite some difference in modelling. Note that for the first pair of modes, the forward whirling mode has a lower frequency than the corresponding backward whirling mode.

4.4. CARDAN DRIVE SHAFT

The last example is the dynamic analysis of a flexible drive shaft connected by two universal (or Cardan, or Hooke's) joints. The input and output shaft are assumed rigid, parallel and rigidly supported in lateral direction. The drive shaft is mounted in the plane of the input and output shaft under a misalignment angle α. The two

Table I. Eigenvalues (in [rad/s]) of an example rotor system; the results of the present study and those from [26] are given for comparison.

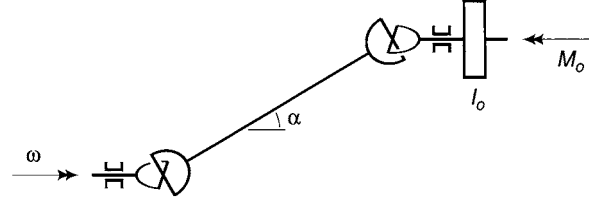| forward/backward	present	from [26]
forward	–7.97 + 223.62 i	–8.04 + 224.13 i
backward	–45.93 + 226.44 i	–45.87 + 226.05 i
backward	–277.46 + 988.02 i	–277.95 + 988.32 i
forward	–205.18 + 1030.30 i	–205.31 + 1031.00 i
backward	–44.45 + 1893.45 i	–44.30 + 1893.95 i
forward	–45.51 + 1921.67 i	–45.77 + 1922.70 i
backward	–158.01 + 4232.13 i	–158.48 + 4233.10 i
forward	–153.39 + 4302.12 i	–153.89 + 4305.32 i

Figure 8. Drive shaft connected by two in-plane universal joints.

universal joints are mounted in such a way that, for a rigid drive shaft, the rotation of the output shaft equals the rotation of the input shaft (see Figure 8).

The misalignment causes an uneven angular velocity of the drive shaft of

$$\omega' = \frac{\cos(\alpha)}{1 - \sin^2(\alpha)\cos^2(\omega t)}\omega, \tag{31}$$

where α is the angle of misalignment. To this unevenness corresponds a variation of the drive shaft torque

$$M_t = \frac{1 - \sin^2(\alpha)\cos^2(\omega t)}{\cos(\alpha)}M_0. \tag{32}$$

In addition, a bending moment is induced in the drive shaft by the applied torque of

$$M_b = \tan(\alpha)\cos(\omega t)\sqrt{1 - \sin^2(\alpha)\cos^2(\omega t)}\,M_0. \tag{33}$$

These results can be found for instance in [27].

The drive shaft of length 1.0 [m] has a solid circular cross section with radius 0.03 [m]. The shaft made of the steel has a mass density of 7850 [kg/m^3], a modulus of elasticity $E = 210 \cdot 10^9$ [N/m^2] and Poisson's ratio of $\nu = 0.3$. The centre line
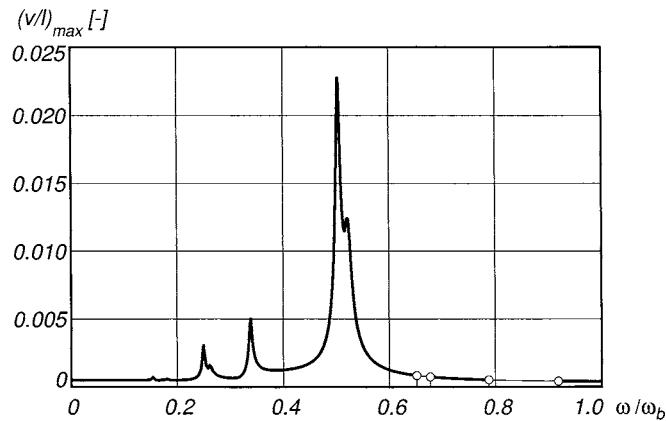
Figure 9. Maximal dimensionless midpoint deflection $(v/l)_{\max}$ for the periodic solution of the drive shaft in the driving speed range of $0 < \omega/\omega_b < 1.0$. The thin lines between circles are the regions of unstable periodic solutions.

of the shaft is assumed inextensible. The material damping (Kelvin–Voigt) is such that the damping of the first eigenmode for small transverse and torsional vibrations is 1% of critical damping. The flexible shaft is modelled by two beam elements (no shear deflection). The misalignment angle α is $\pi/6$ [rad]. At the output side a concentrated moment of inertia $I_o = 0.345555$ [kgm^2] is attached, simulating the reduced moment of inertia of the driven system. The input shaft is driven at a constant angular velocity ω while on the output shaft a constant torque $M_o = 1060.288$ [Nm] is applied, opposed to the direction of rotation, creating a situation of power transmission. The first two bending eigenfrequencies of the undamped, pin jointed shaft are equal due to its symmetry and can be calculated as $\omega_b = 766$ [rad/s]. The concentrated moment of inertia, I_o, is chosen in such a way that, if there is no misalignment, the first torsional eigenfrequency of the undamped shaft (with lumped rotary inertia) equals $1/\sqrt{2}$ times the first bending eigenfrequency.

Figure 9 shows the maximal dimensionless midpoint deflection of the drive shaft in the lateral plane for the periodic solution for different values of the driving speed ω. Resonance occur at about 1/2, 1/3 and 1/4 of the first bending eigenfrequency and not at the eigenfrequency itself. It is interesting to see that the resonances at 1/2 and 1/4 show two peaks close together: the two initially equal eigenmodes in the lateral plane are separated by the torque load in combination with the misalignment. The thin lines between the circles show the regions of unstable periodic solutions, these zones stretch from 0.65 unto 0.68 and from 0.78 unto 0.92. At the boundaries, a pair of complex conjugate characteristic exponents crosses the imaginary axis and Neimark–Hopf bifurcations occur.

The computational effort for calculating, at every individual driving speed, the gross motion, the linearized equations, and the periodic solution was in the order of one second where the effort for determining the stability of the solution, by
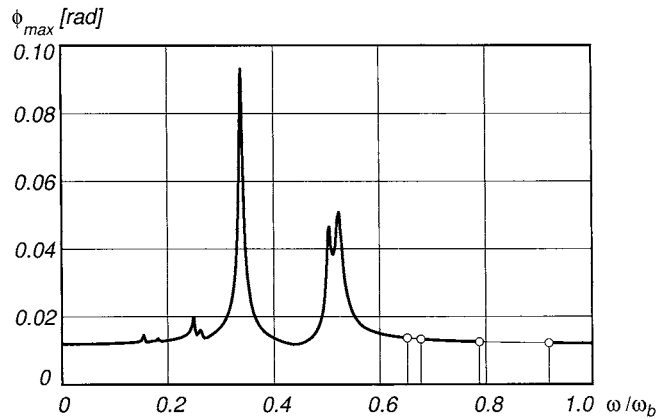
Figure 10. Maximal twist angle $\phi_{\max}$ for the periodic solution of the drive shaft in the driving speed range of $0 < \omega/\omega_b < 1.0$. The thin lines between circles are the regions of unstable periodic solutions.

calculating the characteristic exponents according to (26), was in the order of one minute. Algorithms that calculate only a subset of the eigenvalues would speed up the stability analysis.

Figure 10 shows the maximal twist angle of the shaft for the periodic solution for different values of the driving speed ω. Keeping in mind that the first torsional eigenfrequency equals $1/\sqrt{2}$ times the first bending eigenfrequency ω_b we see that resonance clearly occurs at about 1/2, 1/3 and 1/4 of the first torsional eigenfrequency. Again resonance at the eigenfrequency itself is not present. The resonance at 1/2 of the first bending eigenfrequency is due to the coupling between the bending and the torsion modes. The maximal twist angle at minimum and maximum driving speed is 0.012 [rad], which is about 20% higher than the static twist angle at zero misalignment.

Figure 11 shows the amplitude on a logarithmic scale of the first seven harmonics of the dimensionless midpoint deflection of the shaft for the periodic solution as a function of the driving speed ω in the same range as Figure 9. All even harmonics are zero due to the symmetry of the system. First of all the coupling between bending and torsion is visible in the deflection at zero speed. Second we clearly see all subharmonics resonance with decreasing amplitudes at increasing harmonics.

Figure 12 shows the same presentation for the twist angle. Now all odd harmonics are zero due to the symmetry of the system. Harmonic number zero shows the average twist angle which is about constant over the range of speeds. In the second harmonic we clearly see the resonance at 1/2 of the first bending eigenfrequency together with resonance at 1/2 of the first torsion eigenfrequency. Note the high amplitude contribution of the 4th harmonic at $\omega_b/2$.

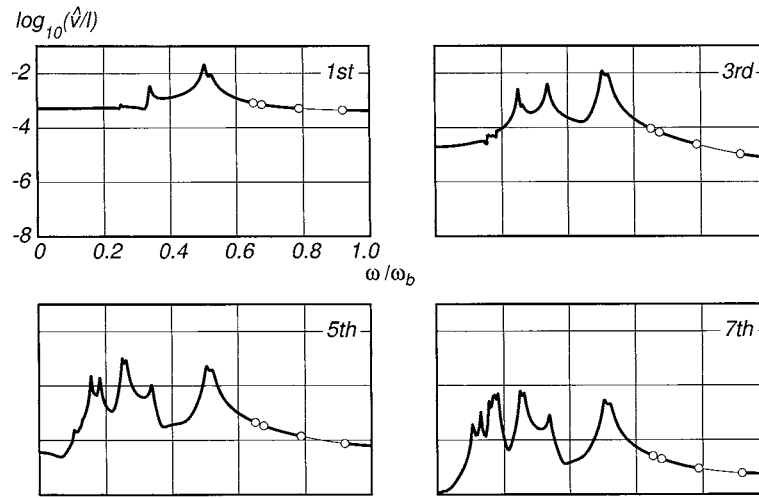All results presented here show hardly any difference with full non-linear results.

Figure 11. The logarithmic amplitude of the first seven harmonics for the dimensionless midpoint deflection v/l of the drive shaft from Figure 9 in the driving speed range of $0 < \omega/\omega_b < 1.0$.
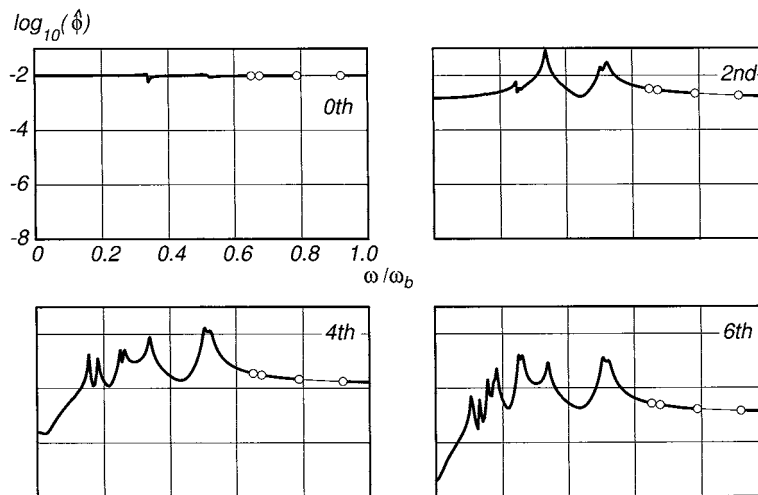

Figure 12. The logarithmic amplitude of the first seven harmonics for the twist angle ϕ of the drive shaft from Figure 10 in the driving speed range of $0 < \omega/\omega_b < 1.0$.

5. Conclusion

A method has been described for the calculation of small elastic vibrations super-imposed on the gross rigid body motion of multibody systems. Periodic solutions as well as transient responses can be determined. In the examples of a pendulum whose support point moves in an elliptic orbit and a slider-crank mechanism with flexible connecting rod, results of the approximate methods compare well with

results from a full non-linear analysis with coupled gross motion and deformation, provided the deformations remain small. A third example has shown how the method can be used to analyse a classical rotor-dynamical model with an independently modelled seal. Finally the application to a drive shaft has shown the practicality for a real engineering problem.

Instability of the solutions generally shows itself by a large increase of the amplitude of the solution, where the linearized solution loses its value. In other cases, as is shown in the last example, the solution may lose its stability in a Neimark–Hopf (secondary Hopf) bifurcation without a large increase in amplitude and with negligible non-linear effects.

The method is computationally efficient in comparison with a full non-linear analysis, especially if the system is stiff, that means, high eigenfrequencies relative to the driving frequency are present, or close to resonance peaks. The calculation of the stability may cost one or two orders of ten more than the determination of the periodic solution itself.

Although the method has been described in connection with a specific multibody formalism, it can be used with any formalism that yields linearized equations in a state space form. Finally, procedures for finding the periodic and transient solutions for the small vibrations in the case of a more general gross rigid body motion, for example a motor driven mechanism with given motor characteristic, are interesting and feasible topics for future work.

References

1. Schiehlen, W., 'Multibody system dynamics: Roots and perspectives', *Multibody System Dynamics* **1**, 1997, 149–188.
2. Shabana, A.A., 'Flexible multibody dynamics: Review of past and recent developments', *Multibody System Dynamics* **1**, 1997, 189–222.
3. Schiehlen, W. (ed.), *Multibody Systems Handbook*, Springer-Verlag, Berlin, 1990.
4. Cleghorn, W.L., Fenton, R.G. and Tabarrok, B., 'Steady-state vibrational response of high-speed flexible mechanisms', *Mechanism and Machine Theory* **19**, 1984, 417–423.
5. Floquet, G., 'Sur les équations différentielles linéaires à coefficients périodiques', *Annales Scientifiques de l'École Normale Supérieure, Sér. 2* **12**, 1883, 47–88.
6. Yakubovich, V.A. and Starzhinskii, V.M., *Linear Differential Equations with Periodic Coefficients*, Nauka, Moscow, 1972 [in Russian]. Translated from Russian by D. Louvish, Israel Program for Scientific Translations, Jerusalem, 1975.
7. Bolotin, V.V., *The Dynamic Stability of Elastic Systems*, Holden-Day, San Francisco, 1964.
8. Friedmann, P.P., 'Numerical methods for the treatment of periodic systems with applications to structural dynamics and helicopter rotor dynamics', *Computers & Structures* **35**, 1990, 329–347.
9. Aannaque, A., Garvey, S., Bennouna, M. and Penny, J., 'Operation of a four-bar mechanism above several critical speeds', *ASME Journal of Vibration and Acoustics* **118**, 1996, 198–203.
10. Ling, F.H. and Wu, X.X., 'Fast Galerkin method and its application to determine periodic solutions of non-linear oscillators', *International Journal of Non-Linear Mechanics* **22**, 1987, 89–98.

11. Cardona, A., Coune, T., Lerusse, A. and Géradin, M., 'A multiharmonic method for non-linear vibration analysis', *International Journal for Numerical Methods in Engineering* **37**, 1994, 1593–1608.
12. Kantorovich, L.V. and Akilov, G.P., *Functional Analysis in Normed Spaces*, Fizmatgiz, Moscow, 1959 [in Russian]. Translated from Russian by D.E. Brown; edited by A.P. Robertson, Pergamon, Oxford, 1964.
13. Schwab, A.L. and Meijaard, J.P., 'Small vibrations superimposed on non-linear rigid body motion', in *Proceedings of DETC'97, 1997 ASME Design Engineering Technical Conferences*, September 14–17, 1997, Sacramento, CA (CD-ROM), ASME, New York, 1997, 7 pp.
14. van der Werff, K. and Jonker, J.B., 'Dynamics of flexible mechanisms', in *Computer Aided Analysis and Optimization of Mechanical System Dynamics*, E. Haug (ed.), Springer-Verlag, Berlin, 1984, 381–400.
15. Jonker, J.B., 'A finite element dynamic analysis of spatial mechanisms with flexible links', *Computer Methods in Applied Mechanics and Engineering* **76**, 1989, 17–40.
16. Meijaard, J.P., 'Direct determination of periodic solutions of the dynamical equations of flexible mechanisms and manipulators', *International Journal for Numerical Methods in Engineering* **32**, 1991, 1691–1710.
17. Jonker, J.B. and Meijaard, J.P., 'SPACAR – Computer program for dynamic analysis of flexible spatial mechanisms and manipulators', in *Multibody Systems Handbook*, W. Schiehlen (ed.), Springer-Verlag, Berlin, 1990, 123–143.
18. Meijaard, J.P., 'Direct determination of periodic solutions of mechanical dynamical systems', *Archive of Applied Mechanics* **64**, 1994, 249–257.
19. Brigham E.O., *The Fast Fourier Transform*, Prentice-Hall, Englewood Cliffs, NJ, 1974.
20. Verhulst, F., *Nonlinear Differential Equations and Dynamical Systems*, 2nd edition, Springer-Verlag, Berlin, 1996.
21. Golub, G.H., and van Loan, C.F., *Matrix Computations*, 3rd edition, The Johns Hopkins University Press, Baltimore, MD, 1996.
22. Hill, G.W., 'On the part of the motion of the lunar perigee which is a function of the mean motions of the sun and moon', *Acta Mathematica* **8**, 1886, 1–36. Previously published by J. Wilson and Son, Cambridge, MA, 1877.
23. Naab, K., and Weyh, B., 'Verallgemeinerte Hill-Matrizen zur direkten Stabilitätsanalyse parametererregter Systeme', *Zeitschrift für angewandte Mathematik und Mechanik* **67**, 1987, T115–T118.
24. Song, J.O. and Haug, E.J., 'Dynamic analysis of planar flexible mechanisms', *Computer Methods in Applied Mechanics and Engineering* **24**, 1980, 359–381.
25. Meijaard, J.P. and Schwab, A.L., 'A systematic approach to the analysis of rotor dynamic systems', in *Proceedings of 10th World Congress on the Theory of Machines and Mechanisms*, Oulu, Finland, June 20–24, T. Leinonen (ed.), Oulu University Press, Oulu, 1999, 1675–1679.
26. Sundararajan, P. and Noah, S.T., 'An algorithm for response and stability of large order non-linear systems–application to rotor systems', *Journal of Sound and Vibration* **214**, 1998, 695–723.
27. Ota, H. and Kato, M., 'Lateral vibrations of a rotating shaft driven by a universal joint (1st report, generation of even multiple vibrations by secondary moment)', *Bulletin of the JSME* **27**, 1984, 2002–2007.